Appl. Phys. A 92, 375–380 (2008)
DOI: 10.1007/s00339-008-4534-y

Applied Physics A
Materials Science & Processing

J.M. MONTES✉
F.G. CUEVAS
J. CINTAS

Porosity effect on the electrical conductivity of sintered powder compacts

Department of Mechanical and Materials Engineering, Escuela Superior de Ingenieros, Universidad de Sevilla, Camino de los Descubrimientos, s/n, 41092 Sevilla, Spain

Received: 2 January 2008/Accepted: 3 April 2008
Published online: 20 May 2008 • © Springer-Verlag 2008

ABSTRACT A new equation for calculating the electrical conductivity of sintered powder compacts is proposed. In this equation, the effective resistivity of porous compacts is a function of the fully dense material conductivity, the porosity of the compact and the tap porosity of the starting powder. The new equation is applicable to powder sintered compacts from zero porosity to tap porosity. A connection between this equation and the percolation conduction theory is stated. The proposed equation has been experimentally validated with sintered compacts of six different metallic powders. Results confirm very good agreement with theoretical predictions.

PACS 72.15.Eb; 72.90.+y; 81.05.Rm; 81.20.Ev

1 Introduction

Modeling the effective properties of porous materials, that is, how their macroscopic properties depend on the porosity, is of extraordinary interest in many scientific areas. These areas are very distinct, and include the study of soil permeability, medication compaction ability, procurement of materials with spongiform structure (known as foams), or fabrication of pieces via powder metallurgy. For these areas, finding equations relating material properties to density or porosity is a crucial problem.

Among the very wide number of effective properties, this work deals with electrical conductivity and its applications in the specific field of powder metallurgy. This is of great importance, as expressions derived in other contexts have been applied to sintered powder compacts. This could be justified when working with high density compacts, i.e., those with very low porosity, but not when the porosity is high. The reason for this is due to the special characteristics of these powdered materials. Table 1 gathers some of the proposed relationships, theoretical or empirical, concerning electrical or thermal conductivity in porous media. Expressions in Table 1 refer to the normalized conductivity (thermal or electrical), which is the ratio of the effective conductivity of the porous material to the conductivity of the bulk or fully dense material.

As can be seen, most of these expressions include some fitting parameter, because the conductivity of sintered parts is closely related to their microstructure. The total porosity level, pore shape, and pore connectivity, as well as material composition and microstructural homogeneity, have a significant influence on the resistivity. It seems that a simple mathematical description as a function of the total porosity, without any empirical coefficients, cannot be derived for predicting the conductivity.

It is intuitive that conductivity increases as porosity decreases. In fact, most expressions in Table 1 verify that the relative conductivity increases from 0 to 1 when the porosity changes from 1 to 0. Nevertheless, these boundary conditions are not valid for powdered materials, as their maximum porosity is always lower than 1. Only the expressions by Loeb [3], McLachlan [8] and Montes et al. [9] satisfy this lower boundary condition, being an application for powdered materials in the high porosities range.

Concerning the expression proposed in [9], in some cases, the results given by the exponent 2 seemed to be too high. This forced a correction in the value of Θ_M, moving it away from the experimentally measured value. On this basis, it seems of interest to review this issue in order to obtain a more satisfactory expression. The new model, proposed in this paper, will be verified with experimentally measured data. The strategy followed in this approach is not based on microstructural aspects measurements, but on a more easily measurable parameter as the powder tap porosity. An alternative method based on the microstructure, using the concept of plain porosity defined by Slesar et al. [11], was carried out by Danninger et al. [12] and Simchi et al. [13]. In these works, besides assessing the influence of the microstructure on the conductivity, a relationship between conductivity and mechanical properties is pursued.

2 Modeling

The electrical conductance (G) of a fully dense material can be calculated from its conductivity value and geometric dimensions. Thus, for a specimen with constant section (S_N) and uniform height (L_N), the electrical conductance is calculated as

$$G = \sigma_0 \frac{S_N}{L_N}\,, \tag{1}$$

where σ_0 is the conductivity of the fully dense material.

Let us consider now a porous specimen with identical geometry and dimensions to the aforementioned specimen.

✉ Fax: +34-954460475, E-mail: jmontes@esi.us.es

Authors	Year	Relative conductivity ($\sigma_R = \sigma_E/\sigma_0$)	Upper boundary condition $\sigma_R \to 1$?	Lower boundary condition $\sigma_R \to 0$?
Maxwell [1]	1873	$\frac{2(1-\Theta)}{2+\Theta}$	$\Theta \to 0$	$\Theta \to 1$
Fricke [2]	1924	$\frac{1-\Theta}{1+a\Theta}$	$\Theta \to 0$	$\Theta \to 1$
Loeb [3]	1954	$(1-b\Theta)$	$\Theta \to 0$	$\Theta \to 1/b$
Murabayashi et al. [4]	1969	$[3(1-\Theta)^c - 1]\left(\frac{1-\Theta}{2+\Theta}\right)$	$\Theta \to 0$	$\Theta \to 1$
Aivazov et al. [5]	1971	$\frac{1-\Theta}{1+d\Theta^2}$	$\Theta \to 0$	$\Theta \to 1$
Meyer [6]	1972	$\frac{e(1-\Theta)}{e+\Theta}$	$\Theta \to 0$	$\Theta \to 1$
Schulz [7]	1981	$(1-\Theta)^f$ (closed porosity)	$\Theta \to 0$	$\Theta \to 1$
McLachlan [8]	1986	$\left(1-\frac{\Theta}{\Theta_c}\right)^{\frac{3}{2}\Theta_c}$	$\Theta \to 0$	$\Theta \to \Theta_c$
Montes et al. [9]	2003	$\left(1-\frac{\Theta}{\Theta_M}\right)^2$	$\Theta \to 0$	$\Theta \to \Theta_M$

TABLE 1 Different expressions for the normalized conductivity (thermal or electrical) as a function of the compact porosity (Θ). Θ_c is the critical porosity (the percolation threshold), Θ_M the tap porosity [10], and the remaining parameters (a, b, c, d, e and f) are material constants

The conductance (G') of this porous specimen (a priori, lower than the one of the fully dense specimen) can be calculated in two different ways. One of them considers the porous material to behave with an effective conductivity, σ_E, lower than σ_0, that is,

$$G' = \sigma_E \frac{S_N}{L_N} . \tag{2}$$

On the other hand, the porous material may be considered to have conductivity σ_0, but the effective cross sectional area for the electrical or thermal flow to pass, as well as the length of the mean path that the flow has to cover, are different (Fig. 1).

Despite both samples in Fig. 1 having the same dimensions, the porous specimen has a lower section for the electrical current to pass through than the fully dense specimen; concretely S_E in the porous sample is less than S_N, because the area corresponding to pores has to be excluded. In a similar way, the path length to be travelled by the electric flow, longitudinally passing through the specimens, will be equal to L_N in the case of the fully dense specimen, and slightly higher, L_E, for the porous specimen, where the flow has to avoid and go around the pores, making the path longer.

S_E and L_E are the effective values of the mean transfer section (smaller than the nominal) and mean effective path (longer than the one corresponding to a fully dense specimen), respectively. The conductance of the porous specimen can be expressed as:

$$G' = \sigma_0 \frac{S_E}{L_E} . \tag{3}$$

Since S_E and L_E are functions of the specimen porosity (Θ), combining (2) and (3) it is possible to obtain an expression

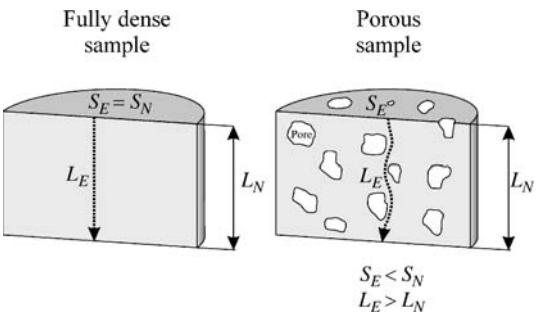

FIGURE 1 Effective area and path for a fully dense and a porous sample

for the effective conductivity, σ_E, as a function of σ_0 and the porosity. Thus, the difficulty is knowing how the effective magnitudes, S_E and L_E, depend on the porosity.

In previous works, the authors have proposed theoretical expressions for the effective section [14, 15] and the effective path [16, 17] of sintered powder compacts. These magnitudes should be sensitive enough to take into account aspects related to the porosity degree and the pores structure. Note that these expressions are related to sintered compacts since only the sintering process ensures the existence of metal–metal contacts between particles, which in turn ensures the continuity of the electric path. If the sintering processes were not carried out, contacts between particles would be interrupted by the oxide surrounding the powder metallic particles. The aforementioned expressions are:

$$S_E = S_N(1 - \Theta/\Theta_M) , \tag{4}$$

$$L_E = L_N \left(\frac{1-\Theta}{1-\Theta/\Theta_M} \right) , \tag{5}$$

where Θ_M is the tap porosity of the starting powders. Essentially, this porosity is that of a powder mass after being vibrated [10]. The tap porosity is very much dependent on particle shape, size and distribution, and, thus, the pore structure after pressing and sintering, depending on the aforementioned parameters, should be to a great extent determined by the value of Θ_M. However, obtaining a clear relationship among those concepts results is quite complex.

It can be verified that $S_E \to S_N$ as $\Theta \to 0$ (fully dense material), and $S_E \to 0$ as $\Theta \to \Theta_M$, when interparticle contacts are points. The limits are different for L_E, which can be seen from (5) since $L_E \to L_N$ as $\Theta \to 0$, but $L_E \to \infty$ as $\Theta \to \Theta_M$. In practice, this represents the non-existence of continuous paths.

By substituting (4) and (5) into (3) the following is obtained:

$$G' = \sigma_0 \frac{S_N}{L_N} \frac{(1-\Theta/\Theta_M)^2}{(1-\Theta)} . \tag{6}$$

In addition, comparing (2) and (6) the next and final expression is obtained:

$$\sigma_E = \sigma_0 \frac{(1-\Theta/\Theta_M)^2}{(1-\Theta)} . \tag{7}$$

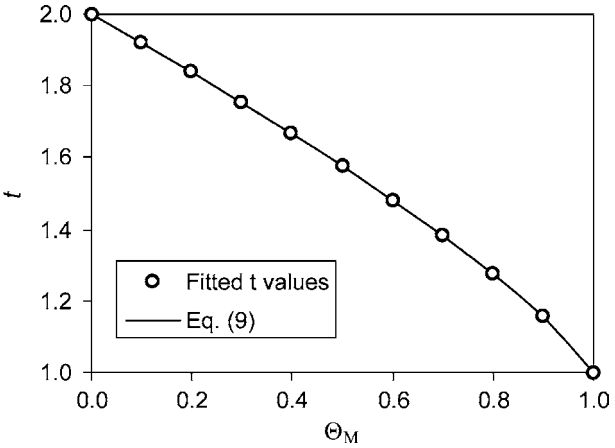

FIGURE 2 Values of t vs. Θ_M optimizing the approximation of (7) and (8). The *continuous line* shows the analytical expression of (9)

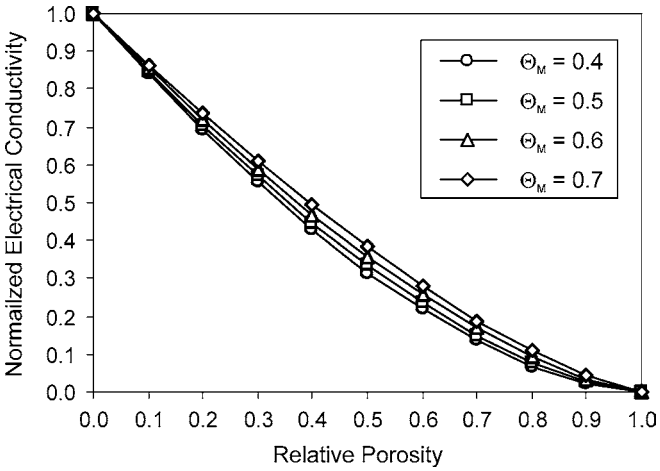

FIGURE 3 Normalized conductivity vs. relative porosity for several values of the tap porosity, Θ_M

It is possible, nevertheless, to make a final change to express σ_E as a function of the relative porosity, defined as $\Theta_R = \Theta/\Theta_M$, instead of the porosity Θ. Effectively, (7) can be rewritten as

$$\sigma_E \approx \sigma_0(1-\Theta/\Theta_M)^t = \sigma_0(1-\Theta_R)^t\,, \tag{8}$$

where the exponent t may be calculated from the expression

$$t = 1 + (1-\Theta_M)^{\frac{4}{5}}\,. \tag{9}$$

The method employed to obtain (9) was as follows: for different values of Θ_M (between 0 and 1), the optimum values of t leading to the best coincidence between (7) and (8) have been calculated by the least squares method (with coefficients of determination better than 0.999). Then, the data cloud of pairs (Θ_M, t) were fitted by an analytical expression relating t and Θ_M, resulting in (9). The excellent, obtained agreement is shown in Fig. 2. Since the approximation degree is noteworthy, as evidenced by the attained coefficient of determination of 0.999, and (8) is simpler than (7), this will be the equation used in this work from this point forward.

Both (7) and (8) satisfy the desired boundary conditions, $\sigma_E \to \sigma_0$ as $\Theta \to 0$, and $\sigma_E \to 0$ as $\Theta \to \Theta_M$, because in this last situation interparticle contacts are points. However, an additional reason for the preference of (8) is its similarity with the percolation theory [18, 19]. In fact, a simple algebraic manipulation of (8) leads to:

$$\begin{aligned}\sigma_E &= \sigma_0(1-\Theta_R)^t \\ &= \sigma_0\left(\frac{\Theta_M-\Theta}{\Theta_M}\right)^t \\ &= \sigma_0\left(\frac{1-\Theta-1+\Theta_M}{\Theta_M}\right)^t\,.\end{aligned} \tag{10}$$

Furthermore, as the term $(1-\Theta)$ coincides, by definition, with the relative density φ, defining $\varphi_c = (1-\Theta_M)$, the following may be obtained:

$$\begin{aligned}\sigma_E &= \sigma_0\left(\frac{\varphi-\varphi_c}{1-\varphi_c}\right)^t \\ &= \frac{\sigma_0}{(1-\varphi_c)^t}(\varphi-\varphi_c)^t\,.\end{aligned} \tag{11}$$

This is

$$\sigma_E \propto (\varphi-\varphi_c)^t\,, \tag{12}$$

which is what the percolation theory predicts [18–20]. According to this theory, φ_c represents the percolation threshold. For the same reason, the tap porosity, Θ_M, also represents such a threshold. A final consideration refers to the exponent value, which reaches values near 2 (but not exactly 2, as happened in [9]), depending on the percolation threshold value. The fact that the exponent t depends on Θ_M means, in the terminology of percolation theory, that the value is not universal. Figure 3 represents the quotient σ_E/σ_0 (σ_R, normalized or relative conductivity) versus the relative porosity (Θ_R), showing the influence of Θ_M on (8).

3 Validation

3.1 *Materials*

Selected powders with different morphologies, all in commercial grade, were studied: AS61 irregular-shaped aluminum powder and 89/11 AK spherical bronze powder from Eckart-Werke; WPL200 and NC 100.24, irregular and spongiform iron powders from QMP and Höganäs AB, respectively; and 4SP 400 spherical and Type 255 filamentary nickel powders from Novamet and Inco, respectively. The very different morphology of the studied powders obtained by scanning electron microscopy (SEM) is shown in Fig. 4.

The selection of two types of iron powders, as well as two of nickel, is made to establish whether the model is sensitive enough to the morphometric characteristics of the powder. Thus, it will be determined whether the parameter Θ_M is good enough to show these differences, even though the two powders have a similar chemical nature. Two iron powders with similar morphometric characteristics have been chosen, as well as two clearly different nickel powders. Finally, aluminum and bronze powders, with similar morphometric characteristics were also studied.

Table 2 lists, for each type of powder, the mean particle radius (r_0) obtained by laser diffraction, and the tap porosity (Θ_M) measured according to MPIF Standards [10]. Essentially, this latter test consists of determining the porosity of

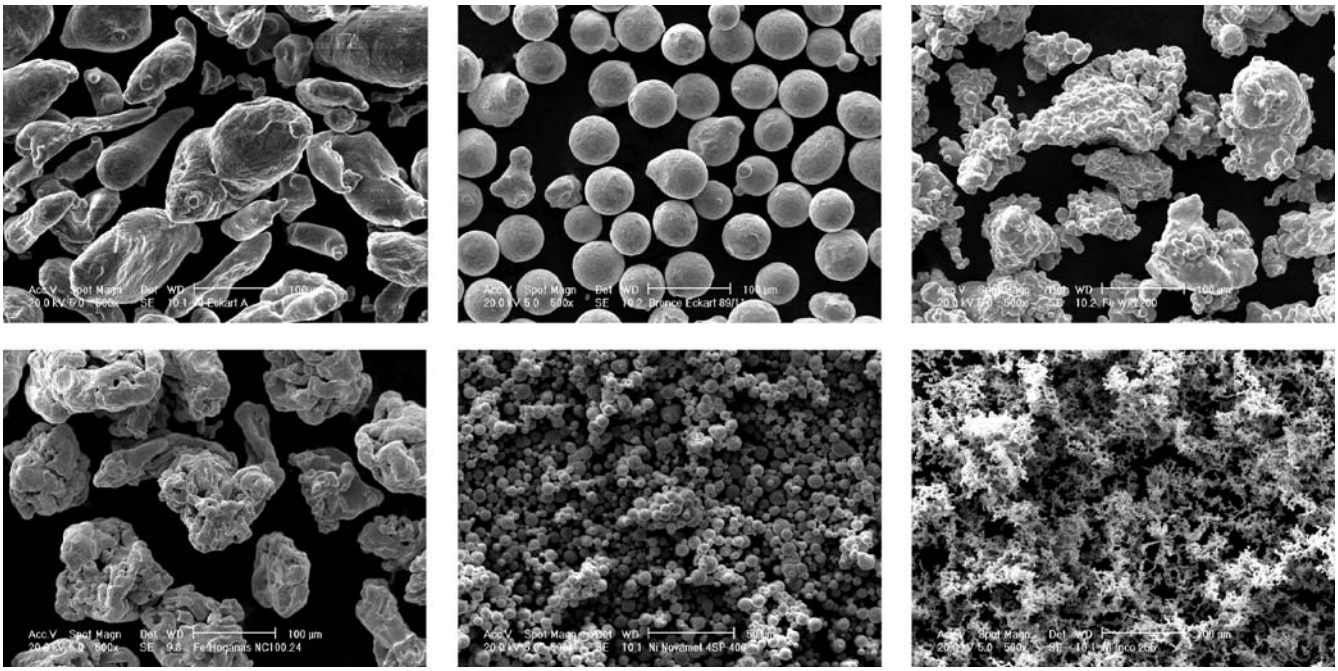

FIGURE 4 From *left* to *right* and from *top* to *bottom*, images of AS61 aluminum, 89/11 AK bronze, WPL 200 iron, NC 100.24 iron, 4SP 400 nickel and Type 255 nickel powders obtained by scanning electron microscopy (SEM)

Powder	r_0 (μm)	Θ_M (exp.)
AS61 aluminum	22.2	0.45
89/11 AK bronze	28.6	0.43
WPL 200 iron	39.2	0.63
NC 100.24 iron	55.6	0.65
4SP 400 nickel	6.6	0.60
T255 nickel	9.4	0.86

TABLE 2 Mean particle radius (r_0) and tap porosity (Θ_M) of studied powders

Powder	Porosity range	Sintering temperature (°C)
AS61 aluminum	0.01–0.32	650
89/11 AK bronze	0.05–0.10	850
WPL 200 iron	0.02–0.43	1150
NC 100.24 iron	0.03–0.44	1150
4SP 400 nickel	0.06–0.37	800
T255 nickel	0.05–0.19	800

TABLE 3 Porosity range of the studied specimens and sintering temperature employed to obtain them

a vibrated powder mass by the measurement of its volume and weight.

The absolute error in the determination of Θ_M, considering the precision of the instruments employed, can be estimated to be ± 0.01, a small value. Nevertheless, during the measuring process, the means and intensity of the vibration could account for a non-controlled increase of the experimental uncertainty. Experimental checks, concerning the vibration effect, lead to an uncertainty range of ± 0.05 for Θ_M, which is still a relatively small value.

3.2 *Experimental procedure*

The electrical conductivity was measured on cylindrical parts, with height of 10 mm and 12 mm diameter, with different porosities. Initially, powders were uniaxially cold compacted according to the desired pressure obtained from the compressibility curve [21]. Porosities ranged from the maximum, allowing for a handleable specimen, to that obtained for a pressure of 1400 MPa, as detailed in Table 3. The compaction was carried out with a uniaxial single action press, in a wall-lubricated fixed-die. The pressing process was followed by 30 min of sintering (1.2×10^5 Pa argon atmosphere) at the temperature indicated in Table 3. Such temperatures were selected after different tests, choosing the lower temperatures allowing a correct sintering with minimum changes in the material microstructure. The final porosity after sintering (Θ) was again measured by weighing and measuring the specimens, and the obtained value is used in later calculations.

Fully dense reference samples of each powder were produced by a double pressing (with intermediate annealing to half of the sintering temperature) and final sintering for 3 h for comparison purposes.

The electric resistance measurements were carried out using the four-point probe technique and a Kelvin bridge (Fig. 5). The resistance was measured several times, at room temperature, changing the probe polarity to remove the thermoelectric effects. Finally, the results were averaged.

From these measurements, whenever the electrode separation s is much lower than the specimen thickness (in our case $s = 2$ mm, vs. a 10 mm specimen height), the electrical conductivity can be calculated as [22]:

$$\sigma_E = (2\pi s R_{measured})^{-1} . \quad (13)$$

The maximum relative error in the conductivity measurement results is lower than 7%. The exception is the Al powders,

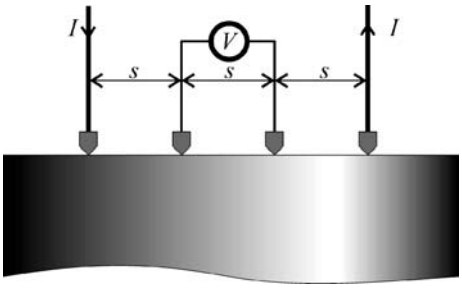

FIGURE 5 Four-point probe scheme for the electrical resistance measurement of a specimen. For convenience, the distance between electrodes is uniform (s). The Kelvin bridge, where electrodes are connected, supplies the quotient V/I (with electrical resistance dimensions, R_{measured}), which is later interpreted

Material	Bulk material conductivity $(\Omega\,\text{m})^{-1}$	Fully dense sample conductivity $(\Omega\,\text{m})^{-1}$
Aluminum	36.63×10^6	34.22×10^6
Bronze 89/11	5.54×10^6	5.37×10^6
Iron	9.59×10^6	8.50×10^6
Nickel	14.03×10^6	12.20×10^6

TABLE 4 Electrical conductivities of bulk materials and fully dense samples, at room temperature

which have a lower R_{measured}. The error in the worst of the cases reaches 20%.

Table 4 gathers the conductivity values of the bulk materials at the measuring temperature ($\sim 25\,^{\circ}\text{C}$) [23], as well as the ones experimentally determined on the fully dense samples. These later values are somewhat lower, probably due to the presence of some residual porosity, contamination introduced by the surface oxides of the powder particles, or traces of other elements.

Considering the values in Table 4, the data cloud corresponding to pairs porosity-effective conductivity was fitted to (8) by the least squares technique. The only fitting parameter was Θ_{M}.

3.3 *Results and discussion*

Figure 6 shows the data clouds corresponding to the pairs (Θ, σ_{E}) and (Θ_{R}, σ_{R}) for each one of the studied powders. In these graphs the fitted theoretical curves are also shown, considering the values of σ_0 obtained for fully dense parts (Table 4), with Θ_{M} as the only fitting parameter. Table 5 gathers the resulting values of Θ_{M} and the coefficients of determination obtained for each of the powders. As can be seen, the achieved fit is quiet acceptable.

The fitted Θ_{M}values are all inside the accepted uncertainty range of ± 0.05, except for the T255 Ni powder. In this case, the obtained value of 0.67 is far from the experimentally measured (0.86). This deviation could be due to the filamentary morphology of this powder, and its great tendency to form agglomerates. This leads to an incorrectly measured tap porosity, which is higher than the actual one. Even a minimum compression (that may be caused by a hand) causes the porosity to abruptly decrease to a value around 0.7 (the value resulting from the fitting process). Thus, it seems that for this type of powder morphology, the tap porosity does not result in

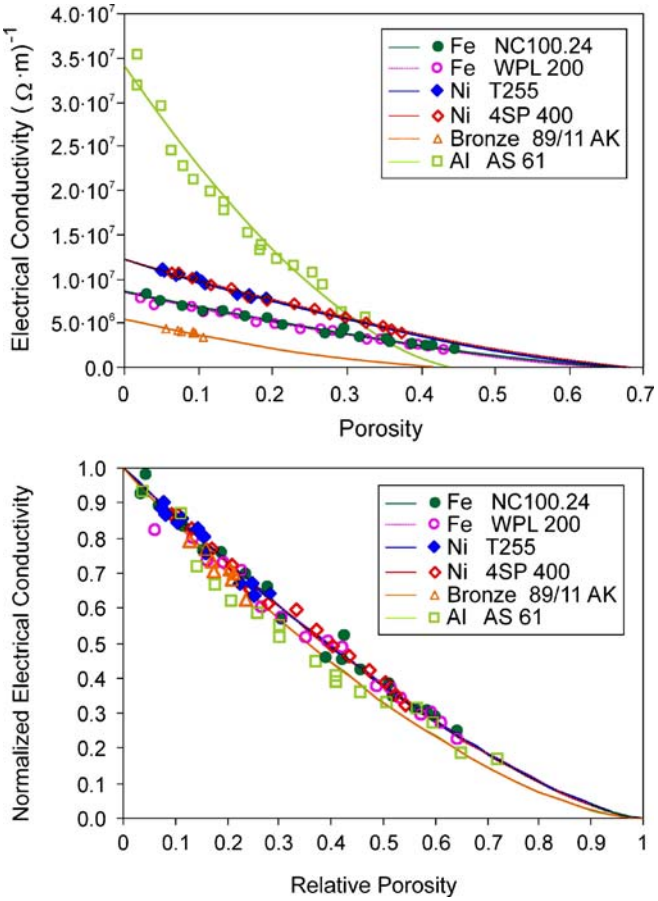

FIGURE 6 Experimental data (*symbols*) and fitted curves (*lines*) according to (8) for the different studied compacts

Powder	Θ_{M} (fitted)	R^2
AS61 aluminum	0.45	0.960
89/11 AK bronze	0.45	0.855
WPL 200 iron	0.67	0.980
NC 100.24 iron	0.69	0.988
4SP 400 nickel	0.69	0.995
T255 nickel	0.67(!)	0.962

TABLE 5 Values of the adjustable parameter (Θ_{M}) in (8), and resulting coefficients of determination after fitting to the experimental data

an adequate parameter. In the rest of the cases, the parameter seems to be perfectly adequate and gathers the morphometric information of the powder.

In order to compare the expression proposed in this paper to those of other authors mentioned in Table 1, the data cloud of the arbitrarily selected NC100.24 Fe powder has also been fitted with such expressions.

In Table 6, parameter p represents the fitting parameter for each one of the expressions. In all fittings, the resistivity value of $8.50 \times 10^6\ (\Omega\,\text{m})^{-1}$, measured on the fully dense sample, has been considered for σ_0. As can be seen, the expression proposed in this work offers the best coefficient of determination. For the first seven expressions in Table 6, the fitting parameter does not have a clear physical meaning. Thus, nothing may be discussed in favor of or against the obtained value. However, it should also be noted that for the expressions reported by McLachlan [8] and Montes et al. [9], the resulting p

Authors	R^2	p
Maxwell [1]	0.579	–
Fricke [2]	0.966	1.83
Loeb [3]	0.979	1.78
Murabayashi et al. [4]	0.985	0.54
Aivazov et al. [5]	0.978	6.52
Meyer [6]	0.966	0.55
Schulz [7]	0.986	2.25
McLachlan [8]	0.947	0.50
Montes et al. [9]	0.987	0.91
This paper	0.988	0.69

TABLE 6 Coefficients of determination and resulting value of the adjustable parameter (p) after fitting the experimentally measured resistivities of the NC100.24 Fe powder with theoretical expressions of several authors

parameter does not give satisfactory results. In the first case, the p value, which represents a certain critical porosity (the percolation threshold), is too low to be identified as the tap porosity (initial), as suggested by Argento et al. [24]. On the other hand, in the second case, p is too high to be tap porosity. If the parameter p is forced (in these two cases) into admissible values (between 0.6 and 0.7), then the coefficients of determination change to 0.896 and 0.765, respectively. Therefore, the expression proposed in this paper represents a better approach in which the fitting parameter acquires a realistic value.

4 Conclusions

A new equation for calculating the effective electrical conductivity of porous sintered materials has been developed. According to this expression, the effective electrical conductivity (σ_E) of a porous sintered compact can be expressed as a function of the fully dense material conductivity (σ_0), its porosity (Θ) and the powders tap porosity (Θ_M):

$$\sigma_E = \sigma_0 (1 - \Theta/\Theta_M)^t ,$$

where $t = 1 + (1 - \Theta_M)^{\frac{4}{5}}$. The validity of this model has been experimentally verified, using sintered compacts of iron, nickel, bronze and aluminum with different porosity levels. Experimental and fitted theoretical values are in very good agreement.

ACKNOWLEDGEMENTS The authors are grateful to FEDER/MCyT, Madrid, for funding this research within the framework of Projects DPI2003-01213 and DPI2005-03711. The authors also wish to thank the technicians J. Pinto, M. Madrid and M. Sánchez for experimental assistance.

REFERENCES

1 J.C. Maxwell, *A Treatise on Electricity and Magnetism* (Dover, New York, 1998)
2 H. Fricke, J. Phys. Rev. **24**, 575 (1924)
3 A.L. Loeb, J. Am. Ceram. Soc. **37**, 96 (1954)
4 M. Murabayashi, Y. Takahashi, T. Mukaibo, J. Nucl. Sci. Technol. **6**, 657 (1969)
5 M.I. Aivazov, I.A. Domashnev, Poroshkovaya Metallurgiya **9**, 51 (1968) [in Russian]
6 R. Meyer, Powder Metall. Int. **4**, 63 (1972)
7 B. Schulz, High Temp. High Press. **13**, 649 (1981)
8 D.S. McLachlan, J. Phys. C Solid State Phys. **19**, 1339 (1986)
9 J.M. Montes, J.A. Rodríguez, E.J. Herrera, Powder Metallurgy **46**, 251 (2003)
10 MPIF Standard 46, Determination of Tap Density of Metal Powders, in *Standard Test Methods for Metal Powders and Powder Metallurgy Products* (MPIF, Princeton, 2002)
11 M. Slesar, E. Dudrova, E. Rudnayova, Powder Metall. Int. **24**, 232 (1992)
12 H. Danninger, G. Jangg, B. Weiss, R. Stickler, Powder Metall. Int. **25**, 170 (1993)
13 A. Simchi, H. Danninger, Powder Metallurgy **45**, 307 (2002)
14 J.M. Montes, F.G. Cuevas, J. Cintas, Mater. Sci. Eng. A **395**, 208 (2005)
15 J.M. Montes, F.G. Cuevas, J. Cintas, Comp. Mater. Sci. **36**, 329 (2006)
16 J.M. Montes, F.G. Cuevas, J. Cintas, J.A. Rodríguez, E.J. Herrerra, The Equivalent Simple Cubic System, in *Trends in Materials Science Research*, ed. by B.M. Caruta (Nova, New York, 2005), pp. 157–190
17 J.M. Montes, F.G. Cuevas, J. Cintas, Granular Mater. **9**, 401 (2007)
18 A.L. Efros, *Physics and Geometry of Disorder. Percolation Theory* (MIR, USSR, 1985)
19 D. Stauffer, A. Aharony, *Introduction to Percolation Theory*, 2nd edn. (Taylor and Francis, London, 1994)
20 P.G. De Gennes, J. Phys. (Paris) **37**, L-1 (1976)
21 MPIF Standard 45, Determination of Compressibility of Metal Powders, in *Standard Test Methods for Metal Powders and Powder Metallurgy Products* (MPIF, Princeton, 2002)
22 J.G. Webster (ed.), *The Measurement, Instrumentation and Sensors Handbook* (CRC, Springer, Berlin Heidelberg New York, 1999)
23 E.A. Brandes (ed.), *Smithells Metals Reference Book*, 6th edn. (Butterworths, London, 1983)
24 C. Argento, D. Bouvard, Int. J. Heat Mass Transf. **39**, 1343 (1996)